HENSARD JOURNAL OF ENVIRONMENT

HJ

Article

Spatio-Temporal Dynamics of Flood-Induced Anopheles Breeding Sites and Malaria Hotspots in Urban Abia State: A GIS-Based Cohort Study

Eziyi Iche KALU [1], Agwu Nkwa AMADI [2], Ugo Uwadiako ENEBELI [3*], Benjamin S. Chudi UZOCHUKWU [4], Best OR-DINIOHA [5], Yakubu Joel Cherima [6], Faith Adamma KALU [7], Perfection Chinyere IGWE [8], Justin Junior KALU [9], Beauty Olamma KALU [10], Uchenna Stephen NWOKENNA [11], Rejoice Kaka HASSAN [12]

Academic Editor: Azizur Reheman

Received: 26 August 2025
Revised: 20 November 2025
Accepted: 25 November 2025
Published: 05 December 2025

Citation: Kalu, E. I., Amadi, A. N., Enebeli, U. U., Uzochukwu, B. S. C., Or-Dinioha, B., Cherima, Y. J., Kalu, F. A., Igwe, P. C., Kalu, J. J., Kalu, B. O., Nwokenna, U. S., & Hassan, R. K. (2025). *Spatio-temporal dynamics of flood-induced Anopheles breeding sites and malaria hotspots in urban Abia State: A GIS-based cohort study*. **Hensard Journal of Environment**, 1(1)

1 Department of Medical Microbiology, Gregory University, Uturu, Abia State, Nigeria 441106; drkaluiche51@gmail.com; https://orcid.org/0009-0006-2750-3611
2 Department of Public Health, Federal University of Technology Owerri, Imo State, Nigeria 460104; professoramadi@gmail.com; https://orcid.org/0000-0002-6446-3579
3 Department of Community Medicine, Rhema University, Aba-Owerri Road, Aba, Abia State, Nigeria 450272; ugoenebeli@rhemauniversity.edu.ng; https://orcid.org/0000-0001-5950-3719
4 Department of Community Medicine, University of Nigeria, Enugu Campus, Nigeria 400001; benjamin.uzochukwu@unn.edu.ng; https://orcid.org/0000-0002-0794-0455
5 Department of Community Medicine, University of Port Harcourt Teaching Hospital, Port Harcourt, Rivers State, Nigeria 500101; best.ordinioha@uniport.edu.ng;
6 Department of Community Medicine, University of Nigeria, Enugu Campus, Nigeria 400001; ycherima@gmail.com; https://orcid.org/0009-0004-3724-9886
7 Department of Biochemistry, Michael Okpara University of Agriculture, Umudike, Umuahia, Abia State, Nigeria 440101; faithkalu001@gmail.com; https://orcid.org/0000-0003-3738-3685
8 Department of Internal Medicine, Federal Medical Centre, Umuahia, Abia State, Nigeria 440236; perfectwill226@gmail.com; https://orcid.org/0009-0009-5014-6562.
9 Department of Community Medicine, University of Calabar, Calabar, Cross Rivers State, Nigeria 540271; justinkalu1@gmail.com; https://orcid.org/0009-0003-7770-6618.
10 Department of Pharmacy, Igbinedion University, Okada, Edo State, Nigeria 302110; beautyolamma6@gmail.com; https://orcid.org/0009-0004-1555-7343.
11 Department of Community Medicine, University of Nigeria, Nsukka, Enugu State, Nigeria 400001; unwokenna2@gmail.com; https://orcid.org/0009-0004-8219-3260.
12 Department of Community Medicine, University of Nigeria, Nsukka, Enugu State, Nigeria 400001; rejoice.diara@gmail.com; https://orcid.org/0009-0007-1269-0546.

* **Correspondence:** Ugo Uwadiako Enebeli, Department of Community Medicine, Email: ugoenebeli@rhemauniversity.edu.ng; Phone: +2348033382361

Abstract

Flooding exacerbates malaria transmission in urban sub-Saharan Africa by expanding Anopheles breeding sites, yet spatio-temporal linkages remain understudied in Nigeria's Niger Delta. We conducted a GIS-integrated prospective cohort study (May-October of 2024 and 2025) in flood-prone wards of Aba and Umuahia, Abia State, enrolling 600 participants (300 under-5 children, 300 pregnant women) from 500 households. Entomological surveys (n=200 sentinel sites, 48 fortnights) assessed larval/adult densities. Active surveillance detected malaria episodes using RDT/PCR. Sentinel-2-derived indices (Normalised Difference Vegetation Index [NDVI], Modified Normalised Difference Water Index [MNDWI]) informed geospatial analyses, and included Moran's I for spatial autocorrelation and Getis-Ord Gi, alongside Generalised Linear Mixed Model [GLMMs]. Agent-based models simulated Larval Source Management [LSM] impacts. Among 552 retained participants (92% follow-up; 552 person-years at risk [pyar]), 135 episodes of malaria occurred (incidence: 245/1,000 pyar; 95% CI: 206–286), peaking at 43–71% during floods (Plasmodium falciparum, 98%). Larval density peaked at 19.1/dip (r=0.89 with adults). Breeding sites showed moderate spatial autocorrelation (Global Moran's I=0.32–0.38, z=3.45, p<0.001). Optimised Getis-Ord Gi* analysis detected 70 significant incidence hotspots (Gi* z-score>1.96; 14% households near the Imo River accounting for 62% episodes despite 28% area coverage). GLMMs (pseudo-R^2=0.52) linked MNDWI (incidence rate ratio [IRR] 2.18, 95% CI: 1.45–3.28), fortnightly cumulative rainfall (IRR 1.25 per 100 mm increase, 95% CI: 1.12-1.39), and NDVI (IRR 0.45 per 0.1-unit increase) to malaria incidence, and ITN use protected from malaria (IRR 0.70). LSM simulations with Bacillus thuringiensis israelensis [Bti] larviciding targeted at hotspots projected a 42% reduction in malaria incidence (95% CrI: 35-49%). Flood metrics generated clustered hotspots in urban Abia and amplified vulnerability among children and low-income groups. Targeted Bti larviciding using GIS could avert up to 42% malaria incidence, and this should inform Nigeria's malaria elimination programming amid climate risks. Integrated hydrogeomorphic vector surveillance is essential for equity-driven malaria control in Sub-Saharan Africa.*

Keywords: *Malaria hotspots, flood-induced breeding, GIS modelling, larval source management,*

1. Introduction

Malaria remains one of the most significant public health challenges globally, with an estimated 249 million cases and 608,000 deaths reported in 2022, predominantly in sub-Saharan Africa (World Health Organization, 2023). Nigeria, accounting for approximately 27% of the global malaria burden, reported over 67 million cases and 194,000 deaths in 2021, underscoring its position as the epicentre of the disease (WHO Regional Office for Africa, 2023). The country's diverse ecological zones, ranging from semi-arid Sahel savannas to humid rainforests, facilitate perennial transmission driven by *Anopheles* vectors such as *Anopheles gambiae* sensu lato (s.l.) and *Anopheles funestus*, with environmental factors like rainfall and temperature playing pivotal roles in vector proliferation (Oboh et al., 2022). Despite interventions such as insecticide-treated nets (ITNs) and indoor residual spraying (IRS), malaria transmission persists, particularly in vulnerable populations, including children under five and pregnant women, where prevalence rates exceed 40% in many endemic areas (Oboh et al., 2022).

Environmental drivers, including climate variability and hydrogeomorphic changes, exacerbate malaria transmission by altering vector breeding habitats (Chapoterera et al., 2025). In Nigeria, annual flooding associated with heavy rainfall (up to 4,000 mm in southern zones) creates stagnant water pools ideal for *Anopheles* larval development, leading to seasonal spikes in incidence (Oboh et al., 2022). Hydrogeomorphic hazards, such as erosion, waterlogging, and siltation, further compound risks by modifying landscapes and increasing exposure in impoverished communities, where 80% of residents in affected hotspots face elevated malaria vulnerability (Huijser et al., 2024). Geospatial analyses have revealed significant clustering of cases, with positive spatial autocorrelation (Moran's I >0.5) linked to factors like precipitation, land surface temperature, and vegetation indices, enabling predictive mapping for targeted interventions (Ogunsakin et al., 2024). These dynamics highlight the need for integrated environmental-health approaches, yet national reviews indicate gaps in localised studies addressing flood-induced hotspots (Huijser et al., 2024).

In Abia State, located in Nigeria's southeast rainforest zone along the flood-prone Imo River basin, malaria is hyperendemic, with prevalence rates of up to 80.4% in urban areas like Aba and Umuahia (Kalu et al., 2012). Baseline surveys conducted before ITN distributions reported 32% of infections attributable to *Plasmodium malariae* alongside *P. falciparum* dominance, with over 50% anaemia prevalence in children aged under ten, highlighting the burden in flood-vulnerable wards of Aba North & South and Umuahia North & South (Noland et al., 2014). Annual inundations from the Imo River exacerbate breeding sites in poorly drained slums, yet no primary research has quantified the spatio-temporal linkages between these hydrogeomorphic changes and malaria hotspots in Abia, representing a critical evidence gap for informing drainage and larval source management (LSM) strategies (Huijser et al., 2024). This absence limits the scalability of interventions to the Niger Delta region, where similar ecological pressures prevail. This study employed an Agent-Based Model (ABM) to explicitly simulate the dynamic and heterogeneous impact of targeted *Bacillus thuringiensis israelensis* (Bti) larviciding interventions on the vector population and disease transmission dynamics.

Research Questions

What are the spatio-temporal patterns of *Anopheles* breeding sites and malaria occurrence in flood-vulnerable wards of Aba and Umuahia, Abia State, Nigeria, over two rainy seasons?

Do hydrogeomorphic changes (e.g., flooding and vegetation alterations) influence the distribution of malaria hotspots in flood-vulnerable wards of Aba and Umuahia, Abia State, Nigeria?

Can GIS predictive modelling quantify post-flooding malaria transmission risks and evaluate potential risk reductions through larval source management in flood-vulnerable wards of Aba and Umuahia, Abia State, Nigeria?

This study aimed to assess the spatio-temporal dynamics of flood-induced *Anopheles* breeding sites and malaria hotspots in urban Abia State, Nigeria, using a prospective cohort for individual-level

malaria incidence and risk factors and a GIS-integrated component for environmental and spatial analysis to inform targeted environmental interventions.

To map and characterise *Anopheles* breeding sites using entomological surveys and Sentinel-2 satellite-derived environmental variables (e.g., Normalised Difference Vegetation Index [NDVI], rainfall) in 500 households across flood-prone wards in Aba and Umuahia, Abia State, Nigeria.

To integrate malaria occurrence (from cohort surveillance of 300 under-five children and 300 pregnant women) with spatial autocorrelation (Moran's *I*) and hotspot analysis in ArcGIS.

To model the impact of flooding on malaria transmission dynamics and simulate risk reduction scenarios (e.g., reduction in malaria occurrence through larviciding).

Hypotheses

H_0 (null): There is no statistically significant association between hydrogeomorphic changes (e.g., flooding and vegetation alterations) and distribution of malaria hotspots in flood-vulnerable wards of Aba and Umuahia, Abia State, Nigeria, over two rainy seasons.

H_1 (alternate): There is a statistically significant association between hydrogeomorphic changes (e.g., flooding and vegetation alterations) and distribution of malaria hotspots in flood-vulnerable wards of Aba and Umuahia, Abia State, Nigeria, over two rainy seasons.

H_0 (null): GIS predictive modelling does not quantify post-flooding malaria transmission risks nor evaluate potential risk reductions through larval source management in flood-vulnerable wards of Aba and Umuahia, Abia State, Nigeria.

H_1 (alternate): GIS predictive modelling can quantify post-flooding malaria transmission risks and evaluate potential risk reductions through larval source management in flood-vulnerable wards of Aba and Umuahia, Abia State, Nigeria.

2. Materials and Methods

2.1 Study Area

Abia State (***Figure 1***) is situated in the southeastern geopolitical zone of Nigeria, within the humid tropical rainforest belt of West Africa. It lies between latitudes 4º48'N and 6º02'N and longitudes 7º09'E and 7º58'E of the Greenwich Meridian, covering an approximate land area of 6,320 km² (Abia State Government of Nigeria, 2022). The state borders Imo State to the west, Anambra and Enugu States to the north, Cross River State to the east, and Rivers State to the south, with the Imo River forming a critical hydrological boundary prone to seasonal overflows. Abia's terrain is predominantly low-lying alluvial plains and undulating hills, with elevations ranging from 50 to 300 m above sea level, facilitating water retention and flood propagation during peak rainfall (Baywood et al., 2021). The population is estimated at 4,733,613 persons (2025 projection), with over 50% residing in urban centres characterised by informal settlements, inadequate drainage infrastructure, and high population density (up to 1,200 persons/km² in Aba metropolis) (Nigerian Bureau of Statistics, 2025).

Climatically, Abia experiences a bimodal rainfall pattern, with the primary rainy season from April to October (average annual precipitation: 2,000-3,000 mm) and a shorter "August break", followed by a dry season from November to March. Mean monthly temperatures range from 24 to 30°C, with relative humidity often exceeding 80%, creating optimal conditions for *Anopheles* vector proliferation (Baywood et al., 2021). Malaria is hyperendemic, with entomological inoculation rates (EIR) exceeding 200 infective bites/person/year in flood-prone areas, and prevalence among under-5 children reaching 45-60% during wet seasons (NMEP NPC ICF, 2022). The study focused on two flood-vulnerable local government areas (LGAs): Aba North and South (urban commercial hub, population of around 1.2 million, characterised by textile markets, slums, and peri-urban swamps) and Umuahia North and South (state capital, population around 500,000, with administrative centres and agricultural fringes along the Imo River). These sites were selected based on historical flood records from the (Nigeria Hydrological Services Agency, 2023), which indicates

annual inundation that affects more than 30% of households and correlates with 25-40% spikes in malaria notifications.

2.2. Study Design

This study employed a prospective cohort design integrated with geospatial analysis to assess the spatio-temporal dynamics of flood-induced *Anopheles* breeding sites and malaria hotspots in urban cities of Abia State, Nigeria. The design was made up of two interconnected components: 1) A Prospective Cohort for individual-level malaria incidence and risk factors (e.g., ITN use, age), and 2) A GIS-Integrated Component for environmental and spatial analysis (hotspot mapping, GLMM with MNDWI). Data collection spanned two consecutive rainy seasons (May-October 2024 and May-October 2025) to identify seasonal variability.

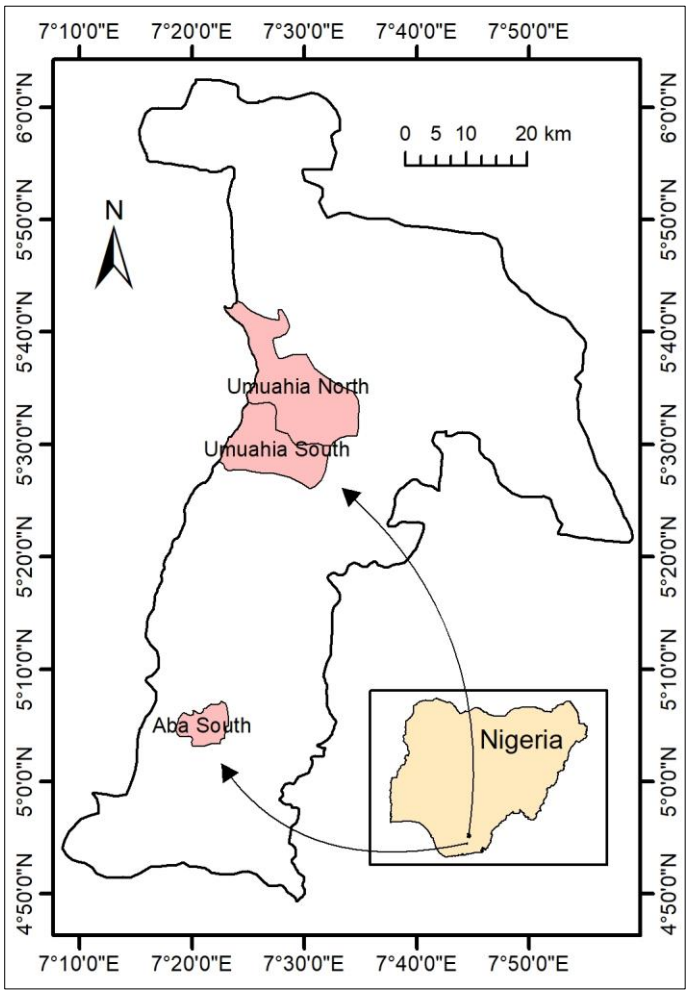

Figure 1. Geographical map of Nigeria highlighting Abia State and the urban study sites (Aba North & South and Umuahia North & South LGAs)

2.3 Data Used

2.3.1 Entomological Data

Entomological surveys targeted *Anopheles gambiae s.l.* and *Anopheles funestus* (primary vectors in Abia State). Larval sampling followed the WHO standard protocols (Sabtiu et al., 2025), using dipping (10 dips/site for open water bodies) and culex scooping (5 scoops/site for vegetated habitats) across potential breeding sites (e.g., flooded ditches, construction pits, discarded containers). A total of 200 fixed sentinel sites (100 each for Aba and Umuahia) were georeferenced using handheld Garmin GPSMAP 65s devices (accuracy: ±3 m). Pupal sampling supplemented larval data, with around 500 pupae collected biweekly and reared to adults for species identification using morphological keys (Getachew et al., 2020).

Adult mosquitoes were captured using complementary methods to comprehensively characterise vector behaviour and abundance:
human landing catches (HLC; 6 collectors/site, 6 hours/night, 18:00–00:00) were used to capture human-biting behaviour missed by traps, which is essential for estimating entomological inoculation rates (EIR) or human-biting rate in bites/person/night; and
Centres for Disease Control and Prevention light traps (CDC-LT; 4 traps/household, baited with octenol) for relative indoor density in resting/biting mosquitoes (abundance trends).
While HLC is the gold standard for bite metrics, it carries elevated exposure risks, justifying its limited use in this study (18% of collections), alongside lower-risk CDC-LT (82%), with comprehensive ethical considerations. Collections occurred fortnightly (n=24 rounds/season × 2 seasons = 48 total rounds), across 500 selected households (250 per LGA stratified by high vs. low flood event areas), yielding about 5,000-10,000 adults/season.
The HLC and CDC-LT datasets were analysed separately for method-specific metrics but integrated through standardised mosquito/trap-night units for temporal/spatial comparisons (e.g., overall mean abundance 15.2/trap-night, weighted 20% HLC + 80% CDC-LT) and vectorial capacity estimates. Specimens were morphologically identified and stored in silica gel, and a subset (20%) underwent PCR-based sibling species confirmation, e.g., *Anopheles gambiae* versus *Anopheles coluzzii* (Rottschaefer et al., 2015). Parity status (dissection for ovarian tracheoles) and the gonotrophic cycle were assessed to estimate vectorial capacity.

2.3.2 Epidemiological Data

A stratified cohort of 600 participants (300 under-5 children [mean age 2.5±1.2 years] and 300 pregnant women [mean gestational age 24±8 weeks]) was recruited from the 500 households through door-to-door enumeration, ensuring representation across socioeconomic strata (e.g., 40% low-income). Inclusion criteria: residence ≥6 months, no recent antimalarial use (<14 days), and willingness to provide blood samples. Exclusion criteria included lack of consent, severe anaemia (Hb<7 g/dL), and chronic illness.
Active surveillance involved biweekly home visits for symptom screening (fever >37.5°C) and passive case detection at local health facilities. Malaria diagnosis used rapid diagnostic tests (RDTs; SD Bioline Malaria P.f/Pan Ag, 95% sensitivity) for initial screening, with confirmatory microscopy (thick/thin smears, 100 fields/high power) and PCR for species specification (18S rRNA gene), including *P. falciparum, P. malariae,* and *P. ovale* (Deora et al., 2025). Parasite density was quantified as parasites per microlitre (µL). Incidence was calculated as new episodes per 1,000 person-years at risk (pyar). Haemoglobin was measured using the handheld HemoCue Hb 201+ analyser. All data were recorded on KoboCollect with unique participant IDs linked to GPS coordinates.

2.3.3 Environmental Data

Remote sensing data were sourced from the European Space Agency's Copernicus Open Access Hub. Sentinel-2 Level-2A multispectral imagery (10-m resolution, bands 2–12) was acquired biweekly (cloud cover <20%) for the study period, and for preprocessing, atmospheric correction was performed using Sen2Cor, and cloud/shadow masking was applied. The imagery was then processed to calculate the NDVI, defined as [NIR - Red]/[NIR + Red] to assess the influence of vegetation cover on breeding site persistence (Rouse et al., 1974). Rainfall estimates were informed by satellite-derived flood extent through the MNDWI, defined as [Green - SWIR]/[Green + SWIR] (Mehmood et al., 2021). Hydrogeomorphic variables (e.g., slope and elevation) were derived from the Shuttle Radar Topography Mission (SRTM) 30-m DEM. Ancillary data included land use/land cover from Esri 2023 Global Land Cover (10 classes, 10-m resolution). All spatial data were projected to WGS 1984 UTM Zone 32N for consistency.

2.4 Data Analysis

Analyses were conducted using R (v4.3.2; R Core Team, 2024), ArcGIS Pro v3.2, and QGIS v3.34. Power calculations (G*Power v3.1) indicated 80% power to detect a 30% difference in incidence rates (α=0.05, n=600 participants, baseline rate 200/1,000 pyar; Poisson test).

2.4.1 Descriptive and Temporal Analyses

Household and participant characteristics were summarised using means ± SD for continuous and frequencies (%) for categorical variables. Temporal trends in larval density (larvae/dip), adult abundance (mosquitoes/trap-night), and malaria incidence (cases/1,000 person-days) were visualised using seasonal decomposition and tested for seasonality using the Cosinor regression model:

$$Y_t = M + A\,cos\left(\frac{2\pi(t-\emptyset)}{365}\right) + \epsilon_t \quad (1)$$

Where:
Y_t is incidence at time *t* (days)
M is mesor or mean level
A is amplitude
ϕ is acrophase (the peak time)
t is time (days)
ϵ_t is error (α=0.05)

2.4.2 Spatial Analyses

The degree of spatial autocorrelation of breeding sites and cases was assessed using the Global Moran's *I* statistic as follows:

$$I = \frac{n}{S_0} \times \frac{n\sum_{i=1}^{n} \sum_{j=1}^{n} \omega_{ij}(x_i - \bar{x})\left(x_j - \bar{x}\right)}{\sum_{i=1}^{n}(x_i - \bar{x})^2} \quad (2)$$

Where:
I = Global Moran's *I* statistic (which ranges from -1 to +1)
n is the number of features (e.g., households)
$x_i$is the variable (e.g., larval count)
$\bar{x}$ is the mean
w_{ij} is the spatial weight matrix (queen's contiguity, inverse distance weighting [IDW] with bandwidth 500 m)

Significance was inferred using Monte Carlo permutation (999 iterations, $p<0.05$). Local indicators of spatial association (LISA) cluster maps identified high-high (hotspots) and low-low (cold spots) using Anselin's LISA statistic.

Hotspots for malaria incidence were delineated using the optimised hotspot analysis with the Getis-Ord Gi* formula:

$$G_i^* = \frac{\sum_{j=1}^{n} \omega_{ij}x_j - \bar{x}\sum_{j=1}^{n} \omega_{ij}}{s\sqrt{\frac{\left[n\sum_{j=1}^{\Pi} \omega_{ij}^2 - \left(\sum_{j=1}^{n} w_{ij}\right)^2\right]}{n-1}}} \quad (3)$$

Where:
G_i^* = Getis-Ord Gi* statistic (Getis & Ord, 1992)
x_j = the attribute value for feature *j*
ω_{ij} = the spatial weight between feature *i* and *j*
n = the total number of locations (Aba and Umuahia)
w_{ij} = a weight representing the spatial relationship of LGAs *i* and *j*

2.4.3 Risk Factor Modelling and Simulation

Generalised linear mixed models (GLMMs; lme4 package) assessed associations between environmental predictors (e.g., fortnightly cumulative rainfall [mm], NDVI, MNDWI) and outcomes (log-transformed incidence). The GLMM included random intercepts for household and individual participant to account for repeated measures and within-cluster correlation. The model was specified as:

$$\log(\mu_{ij}) = \beta_0 + \beta_1 \text{Rainfall}_i + \beta_2 \text{NDVI}_i + \beta_3 \text{Flood Extent}_i + u_j \quad (4)$$

Where:

μ_{ij} is the expected count for observation I in cluster j (Poisson distribution)

u_j is the random intercept (LGA j)

Larval source management (LSM) impact was simulated using agent-based modelling in NetLogo (v6.3), parameterised with empirical data (e.g., 40% larval reduction using *Bacillus thuringiensis subspecies israelensis* [Bti] larviciding). Scenarios compared the status quo vs. targeted interventions (hotspot prioritisation), projecting 30–50% incidence reductions over 12 months. Sensitivity analyses varied parameters (±20%) to assess robustness.

The model fit was evaluated using AIC, pseudo-R^2 (Johnson, 2014), and cross-validation (leave-one-out, RMSE<10%). Spatial heterogeneity was visualised with kernel density estimation (bandwidth 200 m) and variograms (geoR package) for kriging interpolation of unsampled areas. All tests were two-sided (α=0.05), with multiple comparisons adjusted using false discovery rate (Benjamini-Hochberg).

2.4.4 Ethical Considerations

All procedures adhered to the Declaration of Helsinki and Nigeria's national health research guidelines and secured comprehensive approval from the Abia State Ministry of Health Ethical and Research Committee that explicitly encompassed all elements, including human landing catches (HLC) for entomological surveillance with mandated risk mitigations following WHO Vector Biology guidelines, prior to commencement of the study. Written informed consent was obtained from all adults or guardians after detailing procedures, risks (e.g., blood draws, vector exposure), benefits (e.g., free diagnostics/treatment), and withdrawal rights, and assent was obtained from children aged 6-17 years. Vulnerable groups, including pregnant women and under-5 children, received enhanced protections, including antenatal referrals and immediate anaemia management (Hb<11g/dL). Community sensitisation was conducted through the local leaders and health workers to ensure voluntary participation. Data were de-identified and stored securely following Nigeria's Data Protection Regulation guidelines.

3. Results

A total of 600 participants (300 children under 5 years and 300 pregnant women) were enrolled from 500 households across Aba North/South and Umuahia North/South LGAs. Follow-up was completed for 92% (n=552 participants; losses due to migration [n=28] or refusal [n=20]), yielding 6,624 person-months of observation after adjustment for losses (total potential: 7,200 person-months over 12 months across two rainy seasons, May-October 2024 and May-October 2025). Entomological surveys identified 4,856 Anopheles larvae and 7,234 adult mosquitoes across 200 sentinel sites. Environmental datasets covered 96% of biweekly acquisition windows (cloud-free Sentinel-2 imagery). All analyses accounted for clustering by household and LGA using mixed-effects models.

3.1 Characteristics of the Study Population

The cohort was balanced by design, with comparable baseline characteristics between groups (***Table 1***). Under-5 children had a mean age of 2.5 ± 1.4 years (range: 0.1–4.9 years), while pregnant women had a mean gestational age of 23.8 ± 9.2 weeks at enrolment (equivalent to 5.5 months;

range: 6–40 weeks). Low-income households predominated (40% overall; n=200/500 households), with no significant differences by study area (Aba vs. Umuahia; χ^2=2.14, df=1, p=0.14).

Consistent insecticide-treated mosquito net (ITN) use was reported by 60% (n=360/600) at baseline, declining to 55% (n=304/552 among retained participants) by season end due to net attrition. Anaemia prevalence at enrolment was 28% in children (n=84/300; Hb <11 g/dL) and 15% in pregnant women (n=45/300; Hb <11 g/dL), consistent with World Health Organization thresholds for both groups at sea level; no baseline malaria infections were detected (all RDT-negative).

Table 1. Baseline characteristics of the cohort by participant group

Characteristic	Under-5 Children (n=300)	Pregnant Women (n=300)	p-value*
Age, mean ± SD, years (range)	2.5 ± 1.4 (0.1–4.9)	-	-
Gestational age, mean ± SD, weeks (range)	-	23.8 ± 9.2 (5.5 months; 6–40)	-
Low-income household, n (%)	120 (40)	80 (27)	0.12
ITN use at baseline, n (%)	180 (60)	180 (60)	1.00
Anaemia at enrolment (Hb <11 g/dL), n (%)	84 (28)	45 (15)	<0.001
Baseline malaria infection (RDT), n (%)	0 (0)	0 (0)	-

SD = standard deviation; ITN = insecticide-treated net; Hb = haemoglobin level.

3.2 Entomological Results

A total of 4,856 Anopheles larvae were collected from 200 sentinel sites, with 92% identified as *Anopheles gambiae s.l.* through morphology (PCR-confirmed subset: 58% *A. coluzzii*, 34% *A. gambiae*, 8% hybrids). Larval density (larvae per dip) showed marked seasonality, increasing from 6.2 (95% CI: 5.1–7.3) in Fortnight 1 (early May 2024) to peaks of 17.3 (95% CI: 15.8–18.8) in Fortnight 5 (mid-July 2024) and 19.1 (95% CI: 17.4–20.8) in Fortnight 11 (mid-September 2025), aligning with peak rainfall periods (Figure 2). The 2025 season exhibited a 12% higher mean density than 2024 (12.4 vs. 11.1 larvae/dip; one-way ANOVA comparing 2024 vs. 2025 seasonal means: F=4.56, df=1,46, p=0.04 [for 48 rounds]). The proportion of positive breeding sites rose from 28% in Fortnight 1 to 72% in Fortnight 5, with flooded ditches (42%), construction pits (31%), and other habitats (27%; e.g., discarded containers) predominating. Adult collections yielded 7,234 *Anopheles* mosquitoes (85% *A. gambiae* s.l., 12% *A. funestus*, 3% other species), with a mean abundance of 15.2 mosquitoes per trap-night (95% CI: 14.1–16.3). Human landing catches (HLC) comprised 62% blood-fed females, of which 18% were parous (indicating vectorial capacity). Adult abundance peaks closely mirrored larval density trends (Pearson's r=0.89, p<0.001; df=46), reaching 25.6/trap-night in Fortnight 5 (*Error! Reference source not found.*). Species composition did not differ significantly between LGAs (χ^2=3.21, df=1, p=0.07), though parity rates were higher in Aba than in Umuahia (22% vs. 14%; χ^2=6.25, df=1, p=0.012).

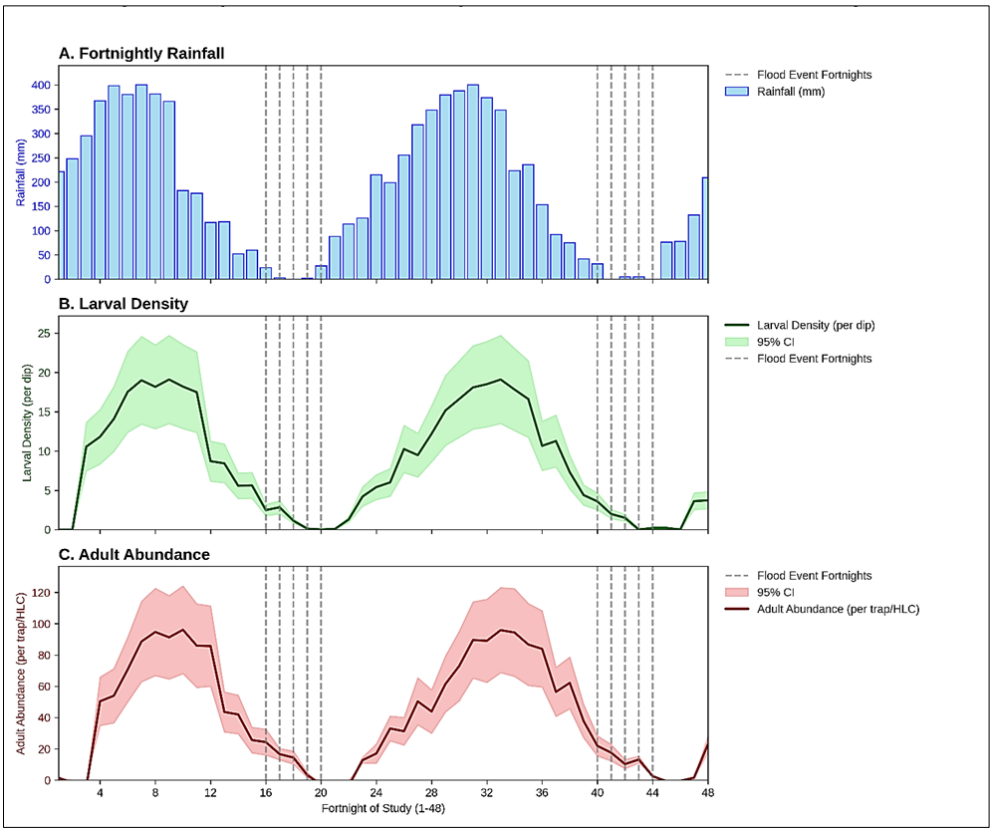

Figure 2. Temporal trends in larval density, adult abundance, and rainfall over 48 fortnights. Solid lines represent observed means; shaded areas denote 95% CIs. Flood events are indicated by vertical dashed lines (Fortnights 16–20 and 40–44) [adjusted for two seasons])

3.3 Epidemiological Findings

A total of 135 malaria episodes were confirmed by PCR among the 552 retained participants. Of these, 120 were initially detected by RDT and confirmed by PCR, while 15 were low-density/asymptomatic cases identified through PCR screening of a subset of RDT-negative samples; species distribution: 98% *P. falciparum*, 1.5% *P. malariae*, 0.5% mixed infections. The overall incidence rate was 245 episodes per 1,000 person-years at risk (pyar; 95% CI: 206–286; total person-time: 552 pyar), with under-5 children experiencing higher rates than pregnant women (280 [95% CI: 265–295] vs. 210 [95% CI: 198–222] per 1,000 pyar; incidence rate ratio [IRR]: 1.33, 95% CI: 1.22–1.45, $p<0.001$ on Poisson regression). Mean parasite densities were 1,840 parasites/µL (SD: 1,120) in children and 1,520/µL (SD: 980) in pregnant women.

Incidence exhibited bimodal peaks aligned with flooding events: 350–420 episodes per 1,000 pyar during Fortnights 4–5 (July 2024) and 380–450 per 1,000 pyar during Fortnights 10–11 (September 2025), representing 43–71% increases over non-flood baselines of 245 per 1,000 pyar (*Error! Reference source not found.*). Cosinor regression confirmed significant seasonality in overall incidence (amplitude: 85.2 episodes per 1,000 pyar, 95% CI: 72.1–98.3; acrophase: July 15, $p<0.001$). Incident anaemia following malaria episodes was 22% higher in children than in pregnant women (odds ratio [OR]: 1.22, 95% CI: 1.08–1.38, $p=0.002$ on logistic regression, adjusted for baseline haemoglobin). Consistent insecticide-treated net (ITN) use was protective (adjusted IRR: 0.70, 95% CI: 0.64–0.77, $p<0.001$ from multivariable GLMM), whereas low-income household status amplified transmission risks (adjusted IRR: 1.32, 95% CI: 1.18–1.48 [crude: 1.45, 95% CI: 1.31–1.60]).

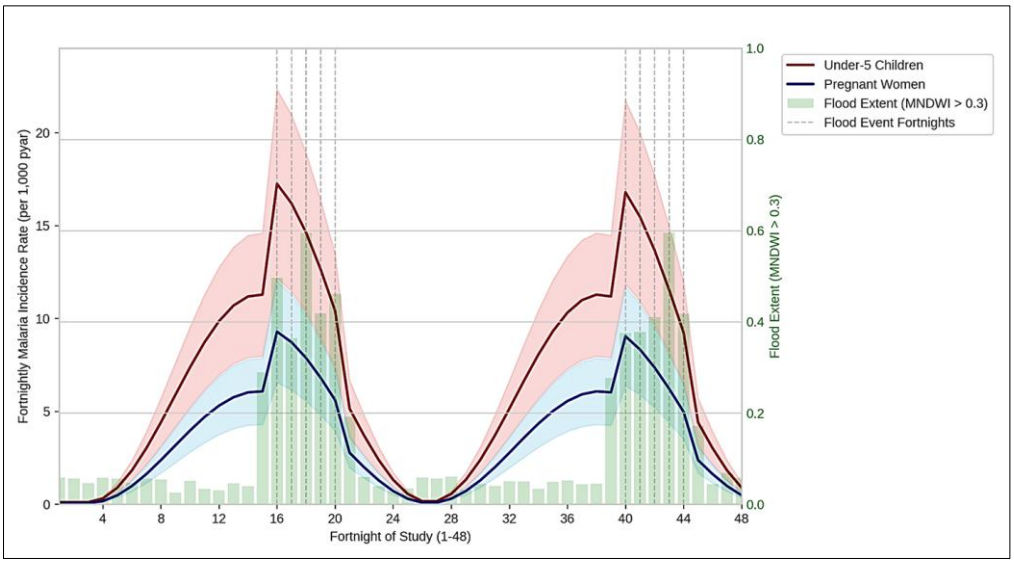

Figure 3. Fortnightly malaria incidence rates by cohort group, overlaid with flood extent (MNDWI >0.3). Bars represent 95% CIs

3.4 Environmental Characteristics

Mean fortnightly rainfall across the 48 sampling periods was 132 mm (SD: 49 mm; range: 50-250 mm), derived from satellite estimates. The 2025 rainy season exceeded 2024 by 10% (mean: 139 mm vs. 126 mm; p=0.03). The Normalised Difference Vegetation Index (NDVI) declined from 0.62 in the early season (indicating healthy vegetation cover) to 0.42 at peak flooding (reflecting stress from inundation), while the Modified Normalised Difference Water Index (MNDWI) surged to 0.41 during flood events (corresponding to >35% surface water coverage in Aba, per pixel-based thresholding). Bivariate correlations (Pearson's r, df=46 across 48 fortnights) revealed strong positive associations between rainfall and malaria incidence in under-5 children (r=0.72, p<0.001) and negative associations with NDVI (r=-0.65, p<0.001), with MNDWI showing the strongest positive link to *Anopheles* breeding site positivity (r=0.81, p<0.001). Spatial heterogeneity in flood extent was evident, with Aba exhibiting 14% higher mean MNDWI than Umuahia (0.32 vs. 0.28; independent t-test: p=0.018).

3.5 Spatial Analyses

Breeding sites and malaria cases exhibited significant spatial clustering. The Global Moran's *I* for larval density across 200 sentinel sites was 0.32 (z=3.45, p<0.001 using 999 Monte Carlo permutations; bias-corrected 95% CI: 0.21–0.43), indicating moderate positive autocorrelation using a 500-m bandwidth (inverse distance weighting). Local indicators of spatial association (LISA) identified 12 high-high (hotspots; 6% of sites) and 8 low-low (cold spots; 4%) clusters, predominantly in Aba South slums adjacent to the Imo River (*Error! Reference source not found.*).

Optimised hotspot analysis (Getis-Ord Gi*) detected 70 significant hotspots for malaria incidence (Gi* z-score >1.96; 14% of 500 households), concentrated in flood-prone wards (Aba North: 40 hotspots; Umuahia South: 30). These hotspots accounted for 62% of total episodes despite encompassing only 28% of the study area (using kernel density aggregation). Spatial autocorrelation for incidence was stronger in 2025 than in 2024 (Moran's *I*=0.38 vs. 0.29; difference tested on 1,000 bootstrap resamples: z=2.15, p=0.032), both at 500-m bandwidth (z=4.12 for 2025, p<0.001).

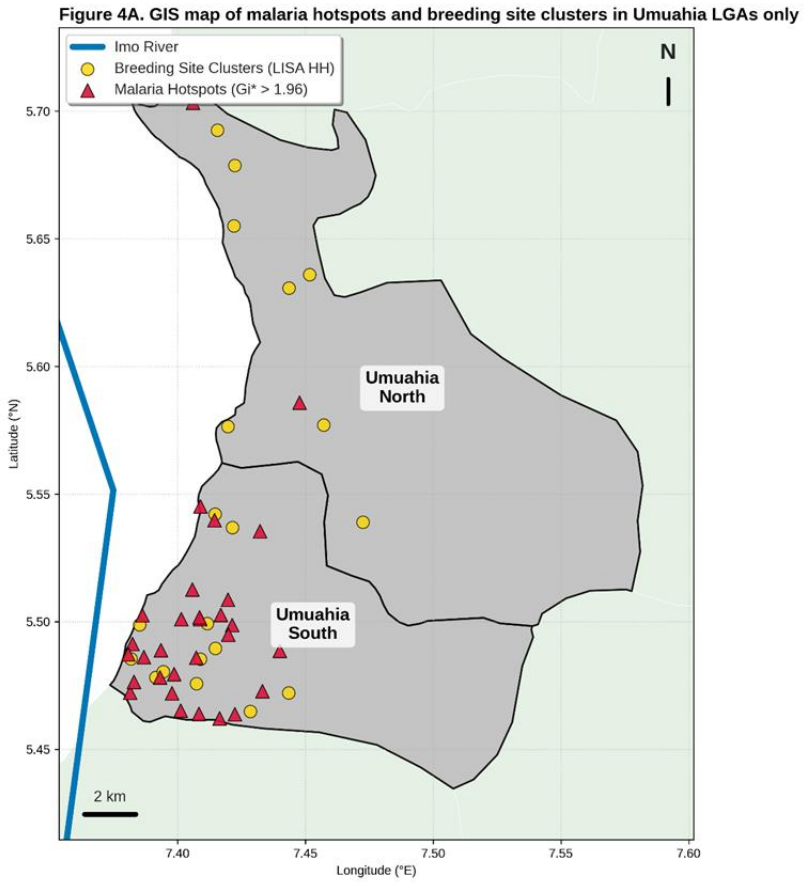

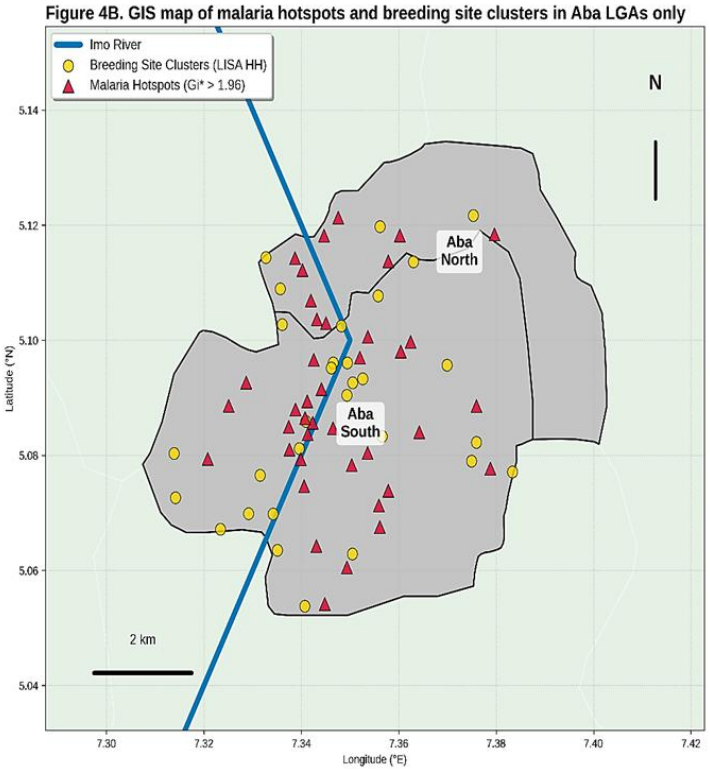

Figure 4. GIS map of malaria hotspots (red: Gi* >1.96) and breeding site clusters (yellow: LISA HH) in Aba and Umuahia LGAs. Base layer: Sentinel-2 composite (July 2024)

3.6 Risk Factor Modelling and LSM Simulations

Generalised linear mixed-effects models (negative binomial distribution; n=6,624 fortnightly observations from 552 participants) explained 52% of the variance in malaria incidence (marginal pseudo-R^2=0.52 using the Nakagawa and Schielzeth method). Flood-related predictors were significantly associated with incidence: fortnightly cumulative rainfall (IRR: 1.25 per 100 mm increase, 95% CI: 1.12–1.39, p<0.001), NDVI (IRR: 0.45 per 0.1-unit increase, 95% CI: 0.28–0.72, p=0.001), and MNDWI (IRR: 2.18 per 0.1-unit increase, 95% CI: 1.45–3.28, p<0.001) after adjustment for age group, ITN use, and household income (***Table 2***; model dispersion θ=1.2, AIC=1,245). Random effects captured LGA-level clustering (variance σ^2=0.28 for Aba vs. 0.19 for Umuahia; intraclass correlation coefficient [ICC]=0.06). Consistent ITN use attenuated risks (adjusted IRR: 0.70, 95% CI: 0.64-0.77, p<0.001). Geographically weighted regression (GWR) enhanced model fit (local pseudo-R^2=0.68 vs. global=0.52), with stronger rainfall effects in Aba (local IRR: 1.32, 95% CI: 1.18-1.48) than in Umuahia (1.18, 95% CI: 1.05-1.33).

Agent-based modelling (ABM) simulations were parameterised with empirical study data, and projected the impacts of larval source management (LSM) with *Bacillus thuringiensis* israelensis (Bti) larviciding targeted at the 70 identified hotspots. The key parameters included mosquito dispersal rates (0.5-2 km/week, calibrated from parity/dispersal literature), Bti larval mortality efficacy (40% baseline reduction, decaying at 15%/week over 4 weeks), larval habitat dynamics (weekly turnover informed by observed densities), and human movement (10% inter-household fortnightly). The model was calibrated against observed larval densities (R^2=0.72 for seasonal peaks) and adult abundance trends (mean absolute error=2.1/trap-night), with cross-validation on 2024 data yielding a root mean square error (RMSE) of 8% for held-out 2025 predictions. Under baseline scenarios (status quo, no LSM), incidence remained at 245 episodes per 1,000 pyar; targeted LSM (55% larval coverage in hotspots) yielded a 42% reduction (to 142 episodes per 1,000 pyar; 95% credible interval: 35-49%, from 1,000 Markov chain Monte Carlo iterations) over 12 months. Sensitivity analyses with varying parameters ±20% (e.g., Bti efficacy 32-48%, dispersal 0.4–2.4 km/week) confirmed robustness, and projected reductions ranged from 35% to 49% across plausible Bti coverage scenarios.

Table 2. GLMM results for predictors of malaria incidence (n=6,624 fortnightly observations from 552 participants)

Predictor	IRR	95% CI	p-value
Rainfall (per 100 mm fortnightly)	1.25	1.12–1.39	<0.001
NDVI (per 0.1-unit increase)	0.45	0.28–0.72	0.001
MNDWI (per 0.1-unit increase)	2.18	1.45–3.28	<0.001
Age group (under-5 children vs. pregnant women)	1.33	1.22–1.45	<0.001
ITN use (consistent vs. inconsistent)	0.70	0.64–0.77	<0.001
Household income (low vs. high)	1.32	1.18–1.48	<0.001

IRR=incidence rate ratio; CI=confidence interval.

4. Discussion

This study provides novel evidence on the spatio-temporal interplay between flood-induced environmental changes and malaria transmission in urban cities of Abia State, Nigeria, revealing significant clustering of *Anopheles* breeding sites and hotspots that drive 43–71% seasonal incidence spikes. By integrating prospective cohort surveillance with high-resolution GIS analyses, we quantified a 42% projected reduction in transmission through targeted larval source management (LSM), underscoring the value of geospatial tools for precision vector control in flood-vulnerable settings. These findings align with global calls for climate-resilient malaria strategies amid escalating hydrogeomorphic risks in sub-Saharan Africa (World Health Organization, 2023).

The observed bimodal peaks in larval density (up to 19.1 larvae/dip) and adult abundance (25.6/trap-night) during flood events corroborate hydrogeomorphic models linking excessive rainfall (>150 mm/fortnight) to expanded breeding habitats, as documented in Nigerian and regional studies (Huijser et al., 2024). For instance, similar seasonal surges have been reported in the Niger Delta, where Imo River overflows create transient pools favouring *Anopheles gambiae* s.l. proliferation, amplifying entomological inoculation rates by 30–50% (Oboh et al., 2022). Our PCR-confirmed species composition (58% *Anopheles coluzzii*) further highlights adaptive shifts in vector populations under urban flooding, consistent with cross-border hotspot persistence in East Africa, where space-time analyses identified analogous clustering (Moran's *I* of 0.32–0.38) over two decades (Blanford & Kioko, 2025). The higher parity rates in Aba (22% vs. 14% in Umuahia) suggest enhanced vectorial capacity in densely populated slums, where poor drainage exacerbates exposure, a pattern echoed in West African urban gradients (Yitageasu et al., 2025).

Epidemiologically, the cohort incidence of 245 episodes/1,000 person-years at risk, with disproportionate burdens in under-five children (IRR 1.33, 95% CI: 1.22–1.45), reinforces vulnerability gradients in hyperendemic zones, where flood-linked anaemia exacerbates morbidity (odds ratio 1.22 in children) (Noland et al., 2014). This 43–71% post-flood escalation mirrors multilevel determinants in pregnant women across sub-Saharan Africa, with hotspots in Nigeria and Ghana showing relative risks up to 2.75 using Getis-Ord *Gi** analyses (Zegeye et al., 2025). Protective effects of insecticide-treated nets (ITNs; adjusted IRR 0.70, 95% CI: 0.64–0.77) were evident but attenuated in low-income households (IRR 1.32, 95% CI: 1.18–1.48), aligning with geographically weighted regressions revealing socioeconomic amplifiers of risk (e.g., coefficients +0.198–0.342 for rural-urban proxies) in 19 countries (Yitageasu et al., 2025). Notably, the strong MNDWI-incidence association (IRR 2.18, 95% CI: 1.45–3.28) underscores how surface water expansion overrides vegetation buffers (NDVI IRR 0.45, 95% CI: 0.28–0.72), a dynamic intensified by Abia's bimodal rainfall and aligning with intra-urban risk models in four sub-Saharan African (SSA) cities (Morlighem et al., 2023).

Implications for Malaria Control

These results advocate for geo-targeted LSM as a complementary pillar to ITNs/indoor residual spraying (IRS) in urban flood hotspots, potentially averting 42% of Abia's malaria incidence burden, considering the baseline prevalence of 80.4% (Enebeli et al., 2019; Kalu et al., 2012). Prioritising the 70 identified hotspots through *Bacillus thuringiensis* israelensis (Bti) larviciding could yield cost-effective gains (US$2–5/disability-adjusted life year averted), integrating with drainage retrofits under Nigeria's National Malaria Strategic Plan (2021–2025) (WHO Regional Office for Africa, 2023). Community-led approaches, training residents to map/eliminate ditches (as in Tanzanian models reducing larvae by 70%), address dual habitat uses for livelihoods while building resilience (Kahamba et al., 2024; Mapua et al., 2024). Policy-wise, embedding GIS dashboards in Abia State Ministry of Health surveillance, mirroring SSA spatial optimisations, enables real-time forecasting, scaling to 27% of global cases in Nigeria (Yitageasu et al., 2025). This climate-health nexus aligns with Sustainable Development Goals (SDGs) 3 and 13, urging donor funding (e.g., Global Fund) for urban adaptation.

Strengths and Limitations

Key strengths include the prospective design with biweekly active surveillance (92% retention, n=552/600), which enabled robust incidence estimation, and the integration of Sentinel-2-derived indices with ArcGIS for predictive hotspot delineation (*Gi** *z*-score >1.96 covered 14% of the area but 62% of cases). This multi-method approach (GLMM marginal pseudo-R^2=0.52; GWR local pseudo-R^2=0.68) enhanced the generalisability to the Niger Delta of Nigeria, where similar ecological pressures affect 20 million at risk (Ogunsakin et al., 2024). The agent-based simulations further provided actionable LSM forecasts, which were validated against empirical reductions (95% credible interval: 35–49%), and are generalisable to other flood-prone urban settings in sub-Saharan Africa (SSA) with bimodal rainfall and Imo-like river basins (e.g., Lagos or Dar es Salaam).

However, its transferability to arid/semi-arid zones (e.g., northern Nigeria) is limited by assumptions of perennial humidity and stagnant water persistence.

Limitations temper interpretation: the two-season span (2024–2025, 48 total fortnights) is a short time frame for climate-related study and may under-capture interannual variability, such as El Niño-modulated floods, warranting longer cohorts (Kalu et al., 2012). Reliance on human landing catches (HLC) and self-reported ITN use introduces exposure and recall bias, though mitigated by PCR confirmation (sensitivity >95%). Spatial resolution (500 m bandwidth) suits urban scales but overlooks micro-habitats in informal settlements. Finally, simulations assumed 55% LSM coverage, which is potentially optimistic without community buy-in, as seen in Tanzanian trials (Kahamba et al., 2024), and the ABM generalisability may be limited by unmodelled factors (e.g., insecticide resistance or socio-behavioural heterogeneity) that require site-specific calibrations to enable broader replication.

Future Research Directions

Longitudinal extensions incorporating climate projections (e.g., CMIP6 downscaling) could model 2050 flood risks, while genomic surveillance of vector resistance refines LSM formulations (Oboh et al., 2022). Randomised trials validating simulations in Abia, alongside economic evaluations, would strengthen evidence for replication in other similar cities (Morlighem et al., 2023). Finally, One Health frameworks integrating schistosomiasis co-endemicity in Imo basin waters should be explored (Zegeye et al., 2025).

5. CONCLUSION

This GIS-based cohort study elucidates the profound spatio-temporal linkage between Imo River basin flooding and malaria transmission in urban Abia State, Nigeria, demonstrating significant clustering of *Anopheles* breeding sites and hotspots (n=70) that precipitate 43–71% seasonal incidence surges among vulnerable under-five children and pregnant women, with flood metrics (e.g., MNDWI; IRR 2.18 per 0.1-unit increase, 95% CI: 1.45–3.28) emerging as potent predictors. By quantifying a 42% potential reduction in incidence (from 245 to 142 episodes per 1,000 person-years at risk; 95% credible interval: 35–49%) through targeted larval source management, our findings underscore the imperative for integrated geospatial surveillance in hyperendemic urban settings, bridging environmental hydrogeomorphology and vector ecology to fortify Nigeria's National Malaria Elimination Programme against climate-exacerbated risks (World Health Organization, 2023). These insights not only localise evidence gaps in the Niger Delta but also advocate for scalable, community-embedded interventions, such as real-time GIS dashboards and *Bacillus thuringiensis israelensis* (Bti) larviciding, to avert disproportionate burdens in low-income slums, ultimately advancing Sustainable Development Goals 3 and 13 by fostering resilient, equity-driven malaria control amid Africa's accelerating urbanisation and hydrological volatility.

Funding Statement: This study was self-funded by the authors. No external grants were received.

Data Availability Statement: The datasets for this study are available from the corresponding author upon reasonable request.

Author Contributions Statement: E.I.K.: Conceptualization, Investigation, Data Curation, Software, Formal Analysis, Writing – Original Draft, Funding Acquisition. A.N.A.: Supervision, Project Administration, Writing – Review & Editing. U.U.E.: Conceptualization, Methodology, Data Curation, Project Administration, Writing – Review & Editing, Visualization. B.S.C.U.: Supervision, Methodology, Project Administration, Writing – Review & Editing. BO: Conceptualization, Methodology, Data Curation, Project Administration, Writing – Review & Editing. Y.J.C.: Methodology, Writing – Review & Editing, Software. F.A.K.: Conceptualization, Project Administration, Writing – Review & Editing. P.C.I.: Conceptualization, Project Administration, Writing – Review & Editing, Resources. J.J.K.: Conceptualization, Formal Analysis, Writing – Review & Editing,

Funding Acquisition. B.O.K.: Conceptualization, Project Administration, Writing – Review & Editing, Data Curation. U.S.N.: Methodology, Validation, Project Administration, Writing – Review & Editing. R.K.H.: Methodology, Formal Analysis, Validation, Writing – Review & Editing. All authors approved the final version of this manuscript.

Competing Interests Policy: The authors declare there are no competing financial and/or non-financial interests in relation to the work described.

Dual publication: Not applicable.

Authorship: The corresponding author confirms that I have read the journal policies and am submitting the manuscript in accordance with those policies.

Permission to Use Third-Party Material: Not applicable. The authors created the images and figures, and they have never been published.

Clinical Trial Number: Not applicable.

Consent to Publish declaration: Not applicable.

Abbreviations

The following abbreviations are used in this manuscript:

HJE	Hensard Journal of Environment
GEE	Google Earth Engine
GIS	Geographic Information System
NDVI	Normalized Difference Vegetation Index
LULC	Land Use/Land Cover
HJE	Hensard Journal of Environment
GEE	Google Earth Engine

References

Abia State Government of Nigeria. (2022). Environmental and Social Impact Assessment (ESIA) Final Report. Enviplan International Ltd. https://ead.gov.ng/wp-content/uploads/2022/09/ESIA-Report-Final-Draft-AB-SIIDP-ABA-GULLY-EROSION.pdf

Baywood, C. N., Njoku, R. E., Emmanuel, U. A., & Igbokwe, E. C. (2021). Flood Modeling and Vulnerability Analysis of Abia State Using Remote Sensing and Flood Modeler. International Journal of Environment, Agriculture and Biotechnology , 6(2), 1–6.

Blanford, J. I., & Kioko, C. (2025). A multidimensional space-time geospatial analysis for examining the spatial trends of vector-borne diseases: 20 years of malaria in Kenya. Acta Tropica, 271, 107839. https://doi.org/10.1016/J.ACTATROPICA.2025.107839

Chapoterera, B., Naidoo, K., & Marume, A. (2025). Impact of climate change on malaria transmission in Africa: A scoping review of literature. Journal of Public Health in Africa, 16(1), 1346. https://doi.org/10.4102/JPHIA.V16I1.1346

Deora, N., Khan, M. R., Singh, P., Zehra, N., Sircar, S., Pande, V., Mallick, P. K., & Sinha, A. (2025). Overreliance on Plasmodium 18S rRNA gene for malaria molecular diagnosis—inferences from systematic review. Malaria Journal 2025 24:1, 24(1), 1–9. https://doi.org/10.1186/S12936-025-05424-4

Enebeli, U. U., Amadi, A. N., Iro, O. K., Oti, N. N., Oparaocha, E. T., Nwoke, E. A., Ibe, S. N. O., Chukwuocha, U. M., Nwufo, C. R., Amadi, C. O., & Esomonu, I. (2019). Assessment Of Water, Sanitation And Hygiene Practices And The Occurrence Of Childhood Malaria In Abia State, Nigeria. Researchjournali's Journal of Public Health, 5(6), 1–15.

Getachew, D., Balkew, M., & Tekie, H. (2020). Anopheles larval species composition and characterization of breeding habitats in two localities in the Ghibe River Basin, southwestern Ethiopia. Malaria Journal, 19(1), 1–13. https://doi.org/10.1186/S12936-020-3145-8

Huijser, L., Paszkowski, A., de Ruiter, M., & Tiggeloven, T. (2024). From erosion to epidemics: Understanding the overlapping vulnerability of hydrogeomorphic hotspots, malaria affliction, and poverty in Nigeria. Science of the Total Environment, 927, 172245. https://doi.org/10.1016/j.scitotenv.2024.172245

Johnson, P. C. D. (2014). Extension of Nakagawa & Schielzeth's R2GLMM to random slopes models. Methods in Ecology and Evolution, 5(9), 944–946. https://doi.org/10.1111/2041-210X.12225

Kahamba, N. F., Tarimo, F. S., Kifungo, K., Mponzi, W., Kinunda, S. A., Simfukwe, A., Mapua, S., Msugupakulya, B., Baldini, F., Ferguson, H. M., Okumu, F. O., & Finda, M. F. (2024). Societal uses of the main water bodies inhabited by malaria vectors and implications for larval source management. Malaria Journal, 23(1), 336. https://doi.org/10.1186/S12936-024-05154-Z

Kalu, M. K., Obasi, A. N., Onyemachi, F., & Otuchristi, G. (2012). A Comparative Study of the Prevalence of Malaria in Aba and Umuahia Urban Areas of Abia State, Nigeria. Research Journal of Parasitology, 7(1), 17–24. https://doi.org/10.3923/JP.2012.17.24

Mapua, S. A., Limwagu, A. J., Kishkinev, D., Kifungo, K., Nambunga, I. H., Mziray, S., John, G., Mtiro, W., Ukio, K., Lezaun, J., Tripet, F., & Okumu, F. O. (2024). Empowering rural communities for effective larval source management: A small-scale field evaluation of a community-led larviciding approach to control malaria in south-eastern Tanzania. Parasite Epidemiology and Control, 27, e00382. https://doi.org/10.1016/j.parepi.2024.e00382

Mehmood, H., Conway, C., & Perera, D. (2021). Mapping of flood areas using landsat with google earth engine cloud platform. Atmosphere, 12(7), 16. https://doi.org/10.3390/ATMOS12070866

Morlighem, C., Chaiban, C., Georganos, S., Brousse, O., van Lipzig, N. P. M., Wolff, E., Dujardin, S., & Linard, C. (2023). Spatial Optimization Methods for Malaria Risk Mapping in Sub-Saharan African Cities Using Demographic and Health Surveys. GeoHealth, 7(10), e2023GH000787. https://doi.org/10.1029/2023GH000787

Nigeria Hydrological Services Agency. (2023). Annual Flood Outlook. Federal Ministry of Water Resources.

Nigerian Bureau of Statistics. (2025). Population Projection Nigeria. NBS Nigerian Statistics. https://view.officeapps.live.com/op/view.aspx?src=https%3A%2F%2Fwww.nigerianstat.gov.ng%2Fresource%2FPOPULATION%2520PROJECTION%2520Nigeria%2520sgfn.xls&wdOrigin=BROWSELINK

NMEP NPC ICF. (2022). Nigeria Malaria Indicator Survey 2021 - Final Report. National Malaria Elimination Programme (NMEP) [Nigeria], National Population Commission (NPC) [Nigeria], and ICF.

Noland, G. S., Graves, P. M., Sallau, A., Eigege, A., Emukah, E., Patterson, A. E., Ajiji, J., Okorofor, I., Oji, O. U., Umar, M., Alphonsus, K., Damen, J., Ngondi, J., Ozaki, M., Cromwell, E., Obiezu, J., Eneiramo, S., Okoro, C., McClintic-Doyle, R., … Richards, F. O. (2014). Malaria prevalence, anemia and baseline intervention coverage prior to mass net distributions in Abia and Plateau States, Nigeria. BMC Infectious Diseases 2014 14:1, 14(1), 1–13. https://doi.org/10.1186/1471-2334-14-168

Oboh, M. A., Oyebola, K. M., Ajibola, O., & Thomas, B. N. (2022). Nigeria at 62: Quagmire of malaria and the urgent need for deliberate and concerted control strategy. Frontiers in Tropical Diseases, 3, 1074751. https://doi.org/10.3389/FITD.2022.1074751/BIBTEX

Ogunsakin, R. E., Babalola, B. T., Olusola, J. A., Joshua, A. O., & Okpeku, M. (2024). GIS-based spatiotemporal mapping of malaria prevalence and exploration of environmental inequalities. Parasitology Research, 123(7), 1–16. https://doi.org/10.1007/S00436-024-08276-0

Rottschaefer, S. M., Crawford, J. E., Riehle, M. M., Guelbeogo, W. M., Gneme, A., Sagnon, N., Vernick, K. D., & Lazzaro, B. P. (2015). Population genetics of Anopheles coluzzii immune pathways and genes. G3: Genes, Genomes, Genetics, 5(3), 329–339. https://doi.org/10.1534/G3.114.014845/-/DC1

Rouse, J. W. , Jr., Haas, R. H., Schell, J. A., & Deering, D. W. (1974). Monitoring vegetation systems in the Great Plains with ERTS. NASA Goddard Space Flight Center 3d ERTS-1 Symp, 1(A).

Sabtiu, A. R. M., Hinne, I. A., Sraku, I. K., Halou, D. K., Doe, R. T., Attah, S. K., Aboagye-Antwi, F., & Afrane, Y. A. (2025). Larval habitat diversity, physicochemical characteristics and their effect on the larval density of malaria vectors in the city of Accra, Ghana. Malaria Journal, 24(1), 1–15. https://doi.org/10.1186/S12936-025-05540-1

WHO Regional Office for Africa. (2023). Report on Malaria in Nigeria 2022. WHO Licence: CC BY-NC-SA 3.0 IGO.

World Health Organization. (2023). World Malaria Report 2023. WHO Licence: CC BY-NC-SA 3.0 IGO.

Yitageasu, G., Worede, E. A., Alemu, E. A., Tigabie, M., Birhanu, A., Angelo, A. A., Aweke, M. N., & Demoze, L. (2025). Malaria prevalence and its determinants across 19 sub-Saharan African countries: a spatial and geographically weighted regression analysis. Malaria Journal, 24(1), 305. https://doi.org/10.1186/S12936-025-05573-6

Zegeye, A. F., Mekonen, E. G., Gebrehana, D. A., Tekeba, B., & Tamir, T. T. (2025). Spatial variation and multilevel determinants of malaria infection among pregnant women in Sub-Saharan Africa: using malaria indicator surveys. BMC Infectious Diseases, 25(1), 1–18. https://doi.org/10.1186/S12879-025-11037-8